ICEAIST-24
International Conference on Exploring AI, IOT, Science & Technology-24
ESP Journal of Engineering Technology Advancements / ISSN: 2583-2646

Original Article

Experimental and Numerical Analyses Of Residual Stress Distributions in TIG Welding Process for 304L Stainless Steel

P.Perisamy[1], R.Ramanathan[2], A.Srikanth[3], S.Sibivarma[4], R.Tamilselvan[5]
[1, 2,3,4,5,]*Dept. of Mechanical Engineering M.A.M School of engineering, Siruganur, Tamilnadu, India.*

Abstract: *Residual stresses are produced in weldments due to mismatching and non-uniform distributions of plastic and thermal strains. Attempts were made to analyze the residual stresses produced in the TIG welding process using 2D and 3D finite element analyses. No attempts were made to find the optimum shape of the grooves to minimize the tensile residual stresses in the weldments. In this paper, the effect of geometry configurations on the residual stress distributions are predicted from the 3D computer analysis using a thermoelastoplastic constitutive equation and compared with the X-ray diffraction method. In this study, the effects of conduction, radiation and convection due to both air and inert gas flow rate are considered. Heat capacity, thermal conductivity, elastic modulus, yield stress and other material properties are assumed to be temperature dependent. The effects of the fluid flow, plasticity and external constraint on the residual stress distributions are also considered. Simulation results show that the peak of the tensile residual stress obtained for the u-grooved configuration is less than that predicted for the v-grooved configurations. The predicted residual stresses are in good agreements with those obtained by the X-ray diffraction experiments. It is also shown that the magnitude of the transverse residual stresses increases about threefold if mechanical constraints are applied. The constrained structure also produces less distortion than the un-constrained structure. The best agreement between the residual stress distributions and the X-ray experiments is obtained using the kinematic and isotropic hardening constitutive equations.*

Keywords: *TIG Welding (GTAW), 304L Stainless Steel, Residual Stress Distribution, Experimental Analysis, Numerical Analysis, Finite Element Analysis (FEA)*

INTRODUCTION

Residual stresses and distortions can cause major problems in the welded structures. Residual stresses are produced in the weldments due to mismatching and non-uniform distributions of plastic and thermal strains. As the temperature of the base metal increases, the yield strength decreases and the thermal stress increases. The mismatching (in the weld in general) occurred due to joint geometry and plate thickness. Welding procedures and degree of restraints are also influenced by the residual stress distributions (Taljat et al., 1998). High residual stresses in the regions near the weld can promote brittle fractures, fatigue or stress corrosion cracking. In addition, residual stresses in the base plate may reduce the buckling strength of the structures (Cho et al., 2004). Residual stresses can be measured destructively and non-destructively. For instance, Pang and Pukas (1989) measured stresses destructively by the stress-relaxation methods using strain gauge techniques and Chandra (1985) measured residual stresses non-destructively in the weld bead by X-ray diffraction (XRD) techniques. The XRD is an accurate method to measure the residual stress in a thin surface layer. Finite element methods have also been used to calculate residual stresses (Chang and Teng, 2004). Ueda and Yamakawa (1971) used 2D finite element analysis to calculate the welding resid- ual stress for the first time. McDill et al. (1990) were the first to perform 3D analyses to predict residual stresses in stresses during single pass arc welding. Chang and Teng (2004) performed thermal elasto-plastic analyses using the finite element techniques to obtain the residual stresses in the butt-welded joints. Cho et al. (2004) used finite element analysis to determine the residual stress distributions caused by welding and those produced after post-heat treatment. Teng et al. (2003) assumed the thermo-mechanical behaviors for the

This is an open access article under the CC BY-NC-ND license (https://creativecommons.org/licenses/by-nc-nd/2.0/)

weld materials and considered the effects of welding sequence on the residual stress distributions for a single-pass, multi-pass butt-weld and for a circular patch weld, respectively.Rthe large weldments. Teng and Lin (1998) analytically determined the influence of welding conditions (i.e. travel speed, specimen size, external mechanical constraints and preheat) on resid- ual

Table 1 – Composition ranges for 304 grade stainless steel

Grade	C	Mn	Si	P	S	Cr	Mo	Ni	N
304									
Minimum	–	–	–	–	–	18.0	–	8.0	–
Maximum	0.08	2.0	0.75	0.045	0.030	20.0	–	10.5	0.10

Table 2 – Mechanical properties of 304 grade stainless steel

Grade	Tensile strength (MPa), minimum	Yeild strength 0.2% proof (MPa), minimum	Elongation (% in 50 mm), minimum	Hardness	
				Rockwell B (HRB), maximum	Brinell (HB), maximum
304	515	205	40	92	201

Table 3 – Physical properties of 304 grade stainless steel in the annealed condition

Grade	Density (kg/m³)	Elastic modulus (GPa)	Mean coefficient of thermal expansion (µm/m/°C)			Thermal conduc tivity (W/m K)		Specific heat 0–100 °C (J/kg K)
			0–100 °C	0–315 °C	0–538 °C	At 100 °C	At 500 °C	
304/L/H	8000	193	17.2	17.8	18.4	16.2	21.5	500

1.The experimental tests

In this investigation, grade 304 stainless steel was used. Grade304 is the standard "18/8" stainless. It is the most versatile and most widely used stainless steel, available in a wider range of products, forms and finishes than any other. It has excellent forming and welding characteristics. Grade 304 is readily roll formed into a variety of components for applications in the industrial, architectural, and transportation fields. Grade 304 also has outstanding welding characteristics. Post- weld annealing is not required when welding thin sections. The chemical compositional ranges, mechanical and physical properties for grade 304 stainless steels are given in Tables 1–3,respectively. These data were used in the simulations.

Table 4 lists the various experimental tests carried out in this study. Tables 5 and 6 show the welding parameters employed during welding of three passes and single pass, respectively. The efficiency of the TIG welding process was 70%. The experiments were performed to investigate the effects of plate thickness, weld length, shape and type of groove configuration on the residual stress distributions. In all experiments carried out the E308-XX filler metal were used. The residual stress distributions of all experiments performed were measured by the X-ray diffraction techniques at the positions of 0, 10, 20, 30, 40 and 50 mm distances away from the weld centerlines. All of these experiments were simulated by the finite element method.

Table 4 – Lists of the experimental tests carried out in this investigation

Sample number	Joint type	Groove angle (D)	Number of passes
1	v-Joint	10	1
2	v-Joint	20	3
3	v-Joint	30	3
4	v-Joint	40	3
5	v-Joint	50	3
6	v-Joint	60	3
7	u-Joint	–	3

Table 5 – Welding parameters employed for three pass welding (y = 70%)

Number of passes	Ampere (A)	Voltage (V)	Tungsten electrode diameter (mm)	Filler diameter (mm)	Welding velocity (mm/s)	Gas flow rate (l/min)
1	80–100	15	1.6	1.6	1.5	5
2	150–175	15	2.4	2.4	2	5
3	150–175	15	2.4	2.4	2	5

Analysis model

Tables 4–6 also show the lists of the simulations performed in this study and the corresponded welding parameters. The filler materials characteristics used were similar to those of the base metals (i.e. type 304 austenitic stainless steel).

Thermal and mechanical models

The three-dimensional solid 90 elements were used for the thermal model. The solid 90 element contains 20 nodes. Each node has one degree of freedom. These elements are being suggested for curved boundaries (Miresmaeili, 2005). The ele- ments are suggested to obtain the stable three-dimensional thermal analyses. It is noted in Lu and Kou (1988) that for the TIG welding process, the molten surface is turbulent if the welding current is more than 225 A, so the volume heat gen- eration model should be used to simulate the heat source. If the current is less than 200 A, it is possible to consider the flat molten surface and the main source is suggested to be a surface heat flow model.In this study, following the suggestion of Lu and Kou (1988),when the current was less than 200 A, the surface heat flow model was used. However, the metallographical inspections of the weld zone did not confirm the size of the weld metal zone obtained by the experiments. The weld metal achieved by simulation was less than that obtained by experiments. Therefore, it is inferred that volume heat generation model has also to be included in the analysis. Thus, in this study, the combinations of volume heat generation and surface heat flow models were used to describe the welding heat source. The combinations used were consisted of 20% surface heat flow and 80% volume heat generation. This means that the 20% of the total energy is achieved from the surface heat flow and the 80% of the total energy is obtained from the volume heat generation. The volume heat generation is distributed evenly on the nodes of each element along the weld center-line. The 80% volume heat generation was divided identically (evenly) along all nodes which are located under the welding torch regardless of welding speed (velocity). The surface heat flow is distributed as Gaussian distribution from the tip of the electrode. The Gaussian heat-source distribution is defined as

the thermal analysis, a total of 3900 elements and 300 load steps were used to simulate the complete thermal cycle. Only 31 load steps were required for the weldment to return to its initial temperature. Time increments were automati- cally optimized for each time step by the computer program. The modified Newton–Raphson method was used in each time step for the heat balance iteration.

The convection, radiation and conduction heat transfers are considered in this investigation. The radiation is important at high temperatures and the convection is important at lower temperature and at distances away from the arc. The boundary conditions are assumed as combinations of convection and radiation. The combined thermal conductivity is given by Eq. (2).

$$h = 0.0668T \text{ W/m}^2\,(^\circ\text{C}), \quad 0 < T < 500\,^\circ\text{C}$$
$$h = 0.231T - 82.1 \text{ W/m}^2\,(^\circ\text{C}), \quad T > 500\,^\circ\text{C} \tag{2}$$

Table 6 – Welding parameters employed for single pass welding (y = 70%)

Ampere (A)	250–275
Voltage (V)	15
Tungsten electrode diameter (mm)	3.2
Filler diameter (mm)	3.2
Welding velocity (mm/s)	3.5
Gas flow rate (l/min)	11

Element birth and death

In this study, the technique of element birth and death was used. This option is used for modeling of the process in which part of the material may be added or deleted during the analy-ses such as hole drilling and welding process. Elements which were created initially and those 'born' in the later stages of the analyses were included in the model. In this technique, the software does not remove the dead material during the process. Instead, the software deactivates the materials by multiplying their stiffness to a sufficiently small factor where its default is 10^{-6}. The factor chosen is depended upon the process and is changed due to process.

During the death of the materials, all process variables are set equal to zero. If the dead material is activated, the factor is being removed and the process variables can be obtained for the born materials. It should be noted that in the struc tural analyses the geometrical non-linearity option must be activated in the first loading in order to include the deforma- tion of the material in the subsequent loading. If this matter is not performed, the dead materials are born while the previous deformation is not considered in the analyses.

For the thermal analyses, the dead elements are born according to their properties at their designated temperatures. Their stresses and strains are calculated for the designated temperatures. Under these circumstances, it is possible that the material is born with an initial pre-stress. To solve thisproblem and in order to born the elements with no pre-stresses, the reference data is set to reference temperature rather than the general temperature.

Residual stress measurements by theX-ray diffraction method

X-ray diffraction method employs Bragg's law to estimate the residual strains present in the atomic plans. In this method a monochromatic X-ray beam of sufficient intensity is made to be incident on the atomic planes. The reflected beam from successive planes of atoms is observed. Bragg's law defines thecondition for diffraction through the following equation

$$n\lambda = 2d \sin\theta$$

where λ is the wave length of incident X-rays, θ is the angle between the incident or reflected beam and the reflecting planes, d is the interplanar spacing, and n is the order of reflec- tion (n = 1, 2, 3,.. .). Eq. (13) shows that, if the wavelength of X-rays is known, d can be determined by measuring the angle θ. In the presence of residual stresses, d changes, leading to a shift in X-ray diffraction peaks, which this is a measure of the residual stress.

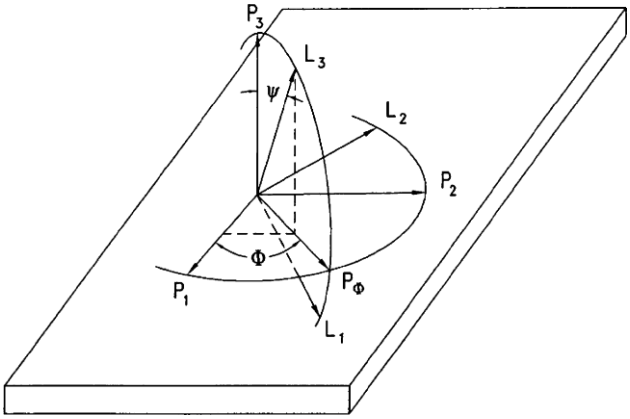

Fig. 1 shows the configuration generally followed for resid- ual stress measurements (Murugan et al., 2001). P_1, P_2 and P_3 refer to three orthogonal directions relative to the sample under investigation and L_1, L_2 and L_3 describe the laboratory or measurement frame of reference. The angles and ϕ definethe relationship between P and L axes; describes the angle between the surface normal (P_3) and the direction of strainbeing measured (L_3); ϕ denotes the angle between one of the principle stress axes (P_1) and the projection of the measured strain direction (L_3) onto the specimen surface. In the widely used sin² method, diffraction measurements are made at several tilt angles .

If d_ϕ is the interplanar spacing in the direction described by the angles ϕ and obtained from the position of diffrac- tion peak for a given '*hk l*' plane, the strain along L_3 may be obtained as

In this study, the X-ray residual stress measurements were made to validate the numerical results. Vanadium filtered Cu Kα radiation of wavelength λ = 1.542 Å was diffracted from the (3 1 1) planes of stainless steel at 2θ = 130°. The sin² method was used to determine residual stress. Seven -angles (0, ±15°, ±30°, ±45°) were used. All the experiments were performed with a 2 mm diameter round collimator. A measurement time of 20 min was found to produce acceptable counting statistics of ±15 MPa. At each location, stress measurements were made in the ϕ = 0°, 45°, and 90° orientations where ϕ = 0° is defined as a direction perpendicular to the weld and ϕ = 90° is a direction parallel to the weld line. Tube voltage used was 40 kV and tube current employed was 30 mA.

Verifications of the simulations

Thermal model verification

The results obtained from the thermal analyses were com- pared with the experimental results. Fig. 2 depicts the typical fusion zone shape obtained by the three-pass welding of stainless steel plates with dimensions of 300 mm length, 100 mm width and 10 mm thickness. Points A, B and C on the fig- ure shows the fusion zones depths and widths at the end of first, second and third pass, respectively. Fig. 3 shows the corresponding fusion zone shape achieved from the numer- ical modeling in the third pass (see point C in Fig. 2). The half widths of the fusion zones obtained from the simu- lations and experiments at end of each pass are listed in Table 8. The agreement between the modeling results and the experiments appears to be very good. The arrow in Fig. 3 indicates the fusion zone. The arrow does not stand for the fluid flow field. The aim of this figure is to illustrate width of the fusion zone and not to show the fluid flow field. Fluid flow simulation in the fusion zone during welding is very difficult.

To study the fusion zone fluid flow, the welding of sample 5 was simulated with and without the inclusion of fluid flow in the fusion zone. With the inclusion of fluid flow model in the fusion zone it was assumed that the heat conduction coefficient at temperatures close to material melting point was two times of the heat conduction coefficient calculated from Eq. (2). The calculated temperature distributions at the mid- length of the weld line for the two conditions are shown in Fig. 4. The temperature distributions are shown for the third pass. Fig. 4a shows the temperature profiles neglecting fluid flow and Fig. 4b shows the temperature profiles when fluid flow is included in the analysis. A comparison of Fig. 4a and b shows that the temperatures obtained at similar distances away from the fusion zones are higher when fluid flow is not considered. In other words, the rate of cooling increases when the fluid flow is considered and experimental results confirms this matter. The size of the half-width fusion zone obtained from the experiments was 7 mm and that obtained from the simulations with the fluid flow, was 7.251 mm (see Table 8). However, the size of the half-width fusion zone when the fluid flow was not considered was 10.9 mm.

Structural model verification

The simulation results from the structural model were com- pared with the experimental results. Two specimens with 1.6 and 10 mm thicknesses were used for verifications. Both weld centerline and at the mid-length of the weld line. On the root side (Fig. 7a), three separated peaks were observed during the three-pass TIG welding process. The maximum tempera- ture obtained was 1887 °C and that occurred during the first pass. The temperature was higher than the material melting point (i.e. 1390 °C). This maximum temperature was located in the fusion zone where melting occurred. In the middle thick- ness (Fig. 7b), two peaks were observed. In this region (point), no welding was performed during the first pass and there- fore one of the peaks was omitted. In other words, during the first pass, there is no material in this area so there is no tem- perature peak. To consider this effect in the simulations, all elements in this region were considered dead during the first pass. Similar conditions were used for the top side of the weld pad (Fig. 7c). In Fig. 7c, the thermal cycle due to the third pass for a typical node located on the top side of the fusion zone is shown. In this area the filler metal is added during the third pass; therefore, the only peak temperature illustrated in Fig. 7c is due to the third pass.

The effect of weld length on the fusion zone peak temperature

In this study, three-dimensional analyses were performed for both thermal and structural models. In most of the previ- ous investigations, the structural models were

carried out in

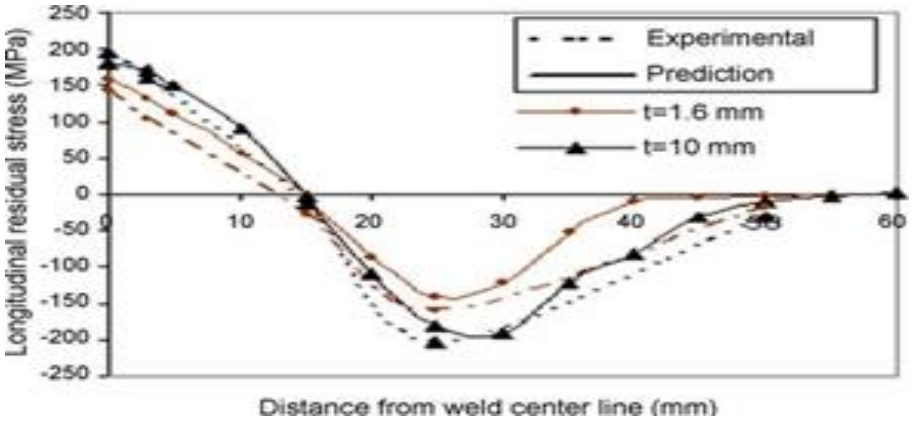

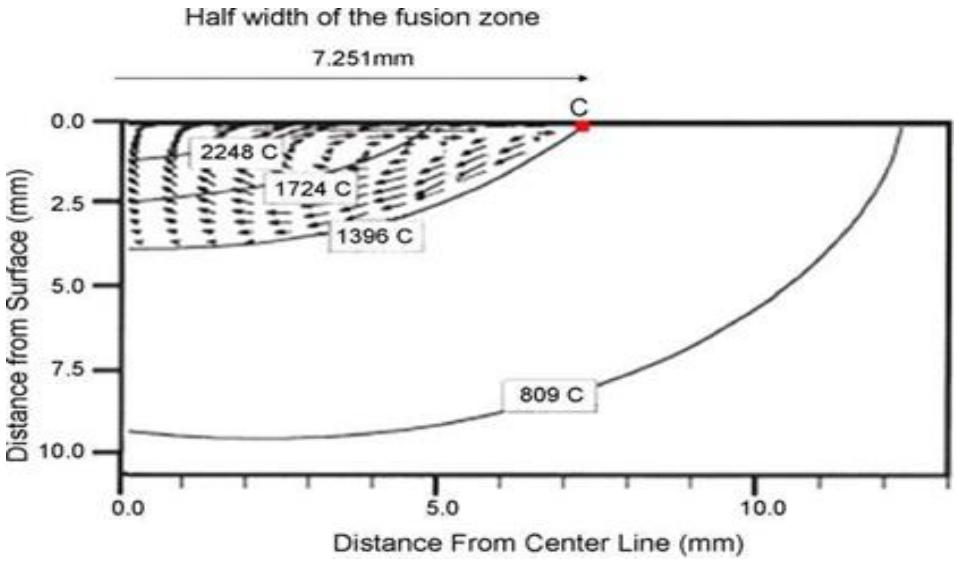

It seems that the maximum temperature at the same distance from the commencement of welding increases after each pass due to preheating of the sample in the earlier pass. The simula- tion results showed the HAZ (heat affected zone) temperature distributions were also affected using by assumptions made above (see Fig. 9). Therefore, in the three-dimensional thermal analysis, the thermal gradients along both the thickness and length are considered.

However, the simulation results performed in this study cannot support these assumptions due to the presents of a thermal gradient and thermal flow along the weld length and thicknesses. Fig. 8 shows the existence of thermal gradi- ents along the weld length. It can be seen that the fusion zone peak temperature increases along the length of the weld. The increase of fusion zone peak temperature by the progression of the weld is attributed to preheating of the materials in the previous steps of welding. This is essential in welding mate- rial with a very long length. Fig. 8 also shows the effect of the number of passes on the fusion zone peak temperature at various points located away from the root side.

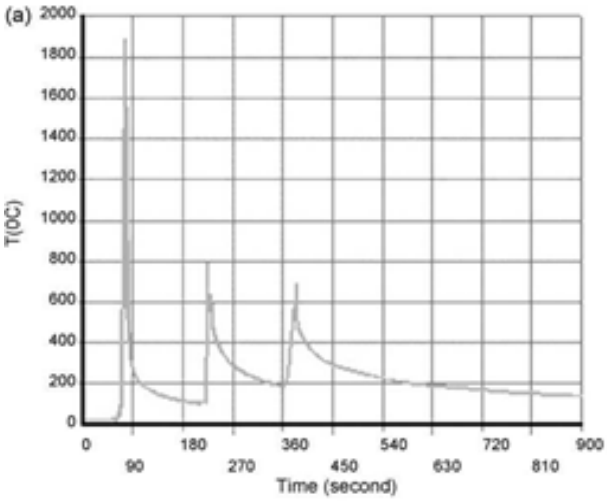
(a)
T(0C)
2000
1800
1600
1400
1200
1000
800
600
400
200
0
0
90
180
270
360
450
540
630
720
810
900
Time (second)

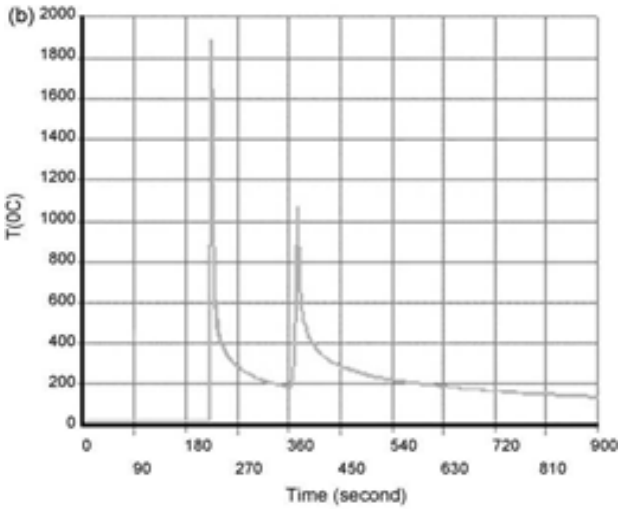
(b)
T(0C)
2000
1800
1600
1400
1200
1000
800
600
400
200
0
0
90
180
270
360
450
540
630
720
810
900
Time (second)

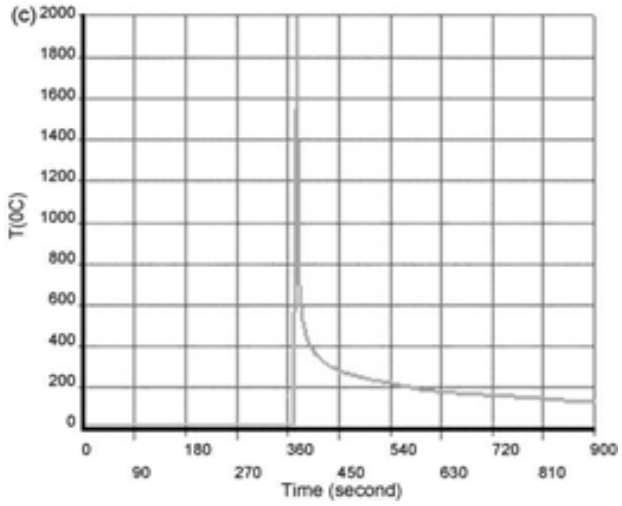
(c)
T(0C)
2000
1800
1600
1400
1200
1000
800
600
400
200
0
0
90
180
270
360
450
540
630
720
810
900
Time (second)

Thermal cycles produced in the sample 5 (see Table 4) at various distances from the root: (a) root side (at mid-length of weld center-line, (b) middle thickness (at mid-length of weld center-line and (c) top side

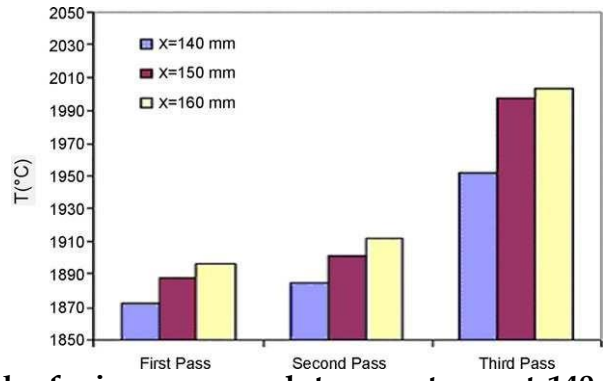

The magnitudes of the fusion zone peak temperatures at 140, 150 and 160 mm distances away form the commencement of welding at different passes in sample 5.3D and thermal modes were performed in 2D. These studies assumed longitudinal symmetry in the thermal models, i.e. heat was assumed to be deposited at the same time along the weld length. Few investigators, however, were investigated 3D thermal models and 2D structural models. The results obtained from the 3D thermal models were mapped into the 2D structural models. These assumptions reduce the size of the FE-model, the CPU-time and the disc memory required for analyses.

Effect of plasticity on the distributions of the residual stress

In this section, the influence of the plasticity on the residual stress distributions is investigated. Two 10 mm thick stain- less steel samples were simulated. The welding was carried out in three passes. Both samples had 50° v-grooved angles (see Tables 4 and 6). Three types of the constitutive equa- tions were used to describe the behavior of the stainless steel plates. These constitutive equations were bilinear isotropic hardening, bilinear kinematic hardening and elastic-perfectly plastic. The corresponding data used is listed in Table 7. The E_T/E ratio in the table refers to the ratio of tangent Mod- ulus (E_T) to Young's Modulus (E) at various temperatures. All materials showed large deformation behavior. The von- Mises yield stress criterion and associated flow rule was used. Fig. 10 shows the residual stress distributions for the kine- matics and isotropic hardening constitutive equations. Note that the magnitude of the peak tensile residual stress obtained using the elastic-perfectly plastic model was smaller than that using the kinematics and isotropic hardening consti- tutive equations. This is attributed to the omission of the hardness effects in the elastic-perfectly plastic constitutive equation. The residual stress distributions obtained using the kinematics and isotropic hardening constitutive equations were in a good agreement with those obtained by the X-ray experiments (see Fig. 10). As the kinematics hardening consti- tutive equations can be used to model the reverse plasticity and Bauschinger effects expected to occur during welding (Brickstad and Josefson, 1998), it was used in the following analyses to describe the behavior of the material.

CONCLUSION

In this study, the effects of the plasticity, external constraint, and groove shapes on the longitudinal and transverse residual stress distributions and on the lengths of the tension

zones were examined numerically and experimentally. The effect of thermal cycling and weld length on the fusion zone peak temperature was investigated.

The main conclusions to be drawn are:

- The minimum longitudinal (and transverse) residual stress and the minimum length of the tension zone were obtained with test specimens containing u-grooves.

- The least tension zone and the minimum tensile longi- tudinal (and transverse) residual stress were produced in specimens containing 50° v-grooves. The minimum von-Mises strains and distortions occurred in the specimenscontaining u-shaped grooves.

- The effect of mechanical constraints on both the 50° u and v grooved specimens was examined. The results showed that the magnitudes of the transverse residual stresses increased about threefold. In addition, the con- strained weld structures had less distortion than the non-constrained weld structures. Mechanical constraints had no major effect on the magnitude of the peak lon- gitudinal residual stress, however the longitudinal stress distribution patterns changed significantly.

- The 3D computer simulations (which included both the thermal and structural models) showed that the fusion zone peak temperature increased along the weld length as the weld progressed.

- The numerical results for residual stress distributions obtained using the kinematic and isotropic hardening con- stitutive equations were in a good agreement with those obtained by the X-ray experiments.

REFERENCE

[1] Naga Ramesh Palakurti, 2023. "*Evolving Drug Discovery: Artificial Intelligence and Machine Learning's Impact in Pharmaceutical Research*" *ESP Journal of Engineering & Technology Advancements* 3(3): 136-147. [Link]

[2] Naga Ramesh Palakurti, 2022. "*AI Applications in Food Safety and Quality Control*" ESP Journal of Engineering & Technology Advancements 2(3): 48-61. [Link]

[3] Chanthati, S. R. (2024). An automated process in building organic branding opportunity, budget Intensity, recommendation in seasons with Google trends data. Sasibhushan Rao Chanthati. https://doi.org/10.30574/wjaets.2024.12.2.0326

[4] Chanthati, Sasibhushan Rao. (2021). How the Power of Machine – Machine Learning, Data Science and NLP Can Be Used to Prevent Spoofing and Reduce Financial Risks. 10.13140/RG.2.2.18761.76640.

[5] Kumar Shukla, Nimeshkumar Patel, Hirenkumar Mistry, 2024." *Securing The Cloud: Strategies and Innovations In Network Security For Modern Computing Environments*" Volume 11, Issue 04 pp. 1786-1796. [Link]

[6] Muthukumaran Vaithianathan, Mahesh Patil, Shunyee Frank Ng, Shiv Udkar, 2024. "*Verification of Low-Power Semiconductor Designs Using UVM*", *ESP Journal of Engineering & Technology Advancements* 4(3): 28-44.

[7] Doctor, A., B. Vondenbusch, and J. Kozak. "Bone segmentation applying rigid bone position and triple shadow check method based on RF data." Acta of Bioengineering and Biomechanics, 13.2 (2011): 3-11.

[8] Jaseem Pookandy, Enhancing Customer Relationship Management with Salesforce: A Comprehensive Review, International Journal of Computer Engineering and Technology (IJCET), 15(4), 2024, pp. 64-84

[9] Muthukumaran Vaithianathan, Mahesh Patil, Shunyee Frank Ng, Shiv Udkar, 2024. "*Energy-Efficient FPGA Design for Wearable and Implantable Devices*" *ESP International Journal of Advancements in Science & Technology (ESP-IJAST)* Volume 2, Issue 2: 37-51.

[10] Jacopo Pianigiani, Michal Styszynski, Atul S Moghe, Joseph Williams, Sahana Sekhar Palagrahara Chandrashekar, Tong Jiang, Rishabh Ramakant Tulsian, Manish Krishnan, Soumil Ramesh Kulkarni, Vinod Nair, Jeba Paulaiyan, Sukhdev S. Kapur, Ashok Ganesan, 2020. *Automation of Maintenance Mode Operations for Network Devices*, US10742501B1. [Link]

[11] Chandrakanth Lekkala, "*Utilizing Cloud – Based Data Warehouses for Advanced Analytics: A Comparative Study*", International Journal of Science and Research (IJSR), Volume 11 Issue 1, January 2022, pp. 1639-1643, https://www.ijsr.net/getabstract.php?paperid=SR24628182046

[12] Julian, Anitha , Mary, Gerardine Immaculate , Selvi, S. , Rele, Mayur & Vaithianathan, Muthukumaran (2024) Blockchain based solutions for privacy-preserving authentication and authorization in networks, *Journal of Discrete Mathematical Sciences and Cryptography*, 27:2-B, 797–808, DOI: 10.47974/JDMSC-1956

[13] Muthukumaran Vaithianathan, 2024. "Digital Signal Processing for Noise Suppression in Voice Signals", IJCSPUB - INTERNATIONAL JOURNAL OF CURRENT SCIENCE (www.IJCSPUB.org), ISSN: 2250-1770, Vol.14, Issue 2, page no.72-80, April-2024, Available: https://rjpn.org/IJCSPUB/papers/IJCSP24B1010.pdf

[14] Muthukumaran Vaithianathan, "Real-Time Object Detection and Recognition in FPGA-Based Autonomous Driving Systems," *International Journal of Computer Trends and Technology*, vol. 72, no. 4, pp. 145-152, 2024. Crossref, https://doi.org/10.14445/22312803/IJCTT-V72I4P119

[15] Muthukumaran Vaithianathan, Mahesh Patil, Shunyee Frank Ng, Shiv Udkar, 2023. "*Comparative Study of FPGA and GPU for High-Performance Computing and AI*" *ESP International Journal of Advancements in Computational Technology (ESP-IJACT)* Volume 1, Issue 1: 37-46. [PDF]

[16] Muthukumaran Vaithianathan, Mahesh Patil, Shunyee Frank Ng, Shiv Udkar, 2024. "*Low-Power FPGA Design Techniques for Next-Generation Mobile Devices*" *ESP International Journal of Advancements in Computational Technology (ESP-IJACT)* Volume 2, Issue 2: 82-93. [PDF]

[17] Dhamotharan Seenivasan, Muthukumaran Vaithianathan, 2023. "*Real-Time Adaptation: Change Data Capture in Modern Computer Architecture*" ESP International Journal of Advancements in Computational Technology (ESP-IJACT) Volume 1, Issue 2: 49-61. [PDF]

[18] Muthukumaran Vaithianathan, Mahesh Patil, Shunyee Frank Ng, Shiv Udkar, 2024. "*Integrating AI and Machine Learning with UVM in Semiconductor Design*" ESP International Journal of Advancements in Computational Technology (ESP-IJACT) Volume 2, Issue 3: 37-51. [PDF]

[19] Chanthati, Sasibhushan Rao. (2021*). A segmented approach to encouragement of entrepreneurship using data science.* World Journal of Advanced Engineering Technology and Sciences. https://doi.org/10.30574/wjaets.2024.12.2.0330, [link]

[20] Patel, N. (2024, March). SECURE ACCESS SERVICE EDGE(SASE): "EVALUATING THE IMPACT OF CONVEREGED NETWORK SECURITYARCHITECTURES IN CLOUD COMPUTING." Journal of Emerging Technologies and Innovative Research. https://www.jetir.org/papers/JETIR2403481.pdf

[21] Vishwanath Gojanur , Aparna Bhat, "Wireless Personal Health Monitoring System", IJETCAS:International Journal of Emerging Technologies in Computational and Applied Sciences,eISSN: 2279-0055,pISSN: 2279-0047, 2014. [Link]

[22] Mistry, H., Shukla, K., & Patel, N. (2024). Transforming Incident Responses, Automating Security Measures, and Revolutionizing Defence Strategies throughAI-Powered Cybersecurity. Journal of Emerging Technologies and Innovative Research, 11(3), 25. https://www.jetir.org/

[23] Aparna Bhat, "Comparison of Clustering Algorithms and Clustering Protocols in Heterogeneous Wireless Sensor Networks: A Survey," 2014 INTERNATIONAL JOURNAL OF SCIENTIFIC PROGRESS AND RESEARCH (IJSPR)-ISSN : 2349-4689 Volume 04- NO.1, 2014. [Link]

[24] Shashikant Tank Kumar Mahendrabhai Shukla, Nimeshkumar Patel, Veeral Patel, 2024." AI BASED CYBER SECURITY DATA ANALYTIC DEVICE", 414425-001, [Link]

[25] Aparna Bhat, Rajeshwari Hegde, "Comprehensive Study of Renewable Energy Resources and Present Scenario in India," 2015 IEEE International Conference on Engineering and Technology (ICETECH), Coimbatore, TN, India, 2015. [Link]

[26] Sarangkumar Radadia Kumar Mahendrabhai Shukla ,Nimeshkumar Patel ,Hirenkumar Mistry,Keyur Dodiya 2024." CYBER SECURITY DETECTING AND ALERTING DEVICE", 412409-001, [Link]

[27] Aparna K Bhat, Rajeshwari Hegde, 2014. "Comprehensive Analysis Of Acoustic Echo Cancellation Algorithms On DSP Processor", International Journal of Advance Computational Engineering and Networking (IJACEN), volume 2, Issue 9, pp.6-11. [Link]

[28] Nimeshkumar Patel, 2022." QUANTUM CRYPTOGRAPHY IN HEALTHCARE INFORMATION SYSTEMS: ENHANCING SECURITY IN MEDICAL DATA STORAGE AND COMMUNICATION", Journal of Emerging Technologies and Innovative Research, volume 9, issue 8, pp.g193-g202. [Link]

[29] Bhat, A., & Gojanur, V. (2015). Evolution Of 4g: A Study. International Journal of Innovative Research in ComputerScience & Engineering (IJIRCSE). Booth, K. (2020, December 4). How 5G is breaking new ground in the construction industry. BDC Magazine.https://bdcmagazine.com/2020/12/how-5g-is-breaking-new-ground-in-the-constructionindustry/. [Link]

[30] Nimeshkumar Patel, 2021." SUSTAINABLE SMART CITIES: LEVERAGING IOT AND DATA ANALYTICS FOR ENERGY EFFICIENCY AND URBAN DEVELOPMENT", Journal of Emerging Technologies and Innovative Research, volume 8, Issue 3, pp.313-319. [Link]

[31] Bhat, A., Gojanur, V., & Hegde, R. (2014). 5G evolution and need: A study. In International conference on electrical, electronics, signals, communication and optimization (EESCO)—2015.[Link]

[32] A. Bhat, V. Gojanur, and R. Hegde. 2015. 4G protocol and architecture for BYOD over Cloud Computing. In Communications and Signal Processing (ICCSP), 2015 International Conference on. 0308-0313. Google Scholar. [Link]